Robust Photoelectrochemical Oxygen Evolution with N, Fe-CoS_2 Nanorod Array

*Jiaying Lu[#], Lejuan Cai[#], Ning Zhang, Bocheng Qiu and Yang Chai**

Department of Applied Physics, The Hong Kong Polytechnic University, Hung Hom, Kowloon, Hong Kong, People's Republic of China. E-mail: ychai@polyu.edu.hk

KEYWORDS: transition-metal dichalcogenides, doping, oxygen evolution reaction, photoelectrochemical, nanorods

ABSTRACT: Photoelectrochemical water splitting is a promising approach to enhance the efficiency of water splitting. However, it is still challenging to develop an efficient oxygen evolution reaction (OER) electrocatalyst that can be coupled with light, due to inefficient light utilization. Here we demonstrate that N, Fe-co-doped CoS_2 (N, Fe-CoS_2) nanorod arrays can act as a highly efficient photo-coupled electrochemical OER catalyst. In dark condition, the doped CoS_2 anode on self-supported stainless steel (SS) mesh shows a small OER overpotential (215 mV) at a current density of 10 mA cm^{-2}, a reduced Tafel slope (43.2 mV dec^{-1}) and negligible activity decay after 10,000 cycles. Upon visible-NIR light illumination, the N-doped anode exhibits superior photoelectrochemical performance due to the enhanced photoresponse, excellent light harvesting ability and promoted interfacial kinetics of charge separation. Our well-designed

photoelectrochemical OER electrode can not only serve as light absorption semiconductor but also the active catalytic site for OER reaction, the electrode composed by single phase can efficiently avoid photo-carrier recombination at the grain boundary. This study provides an insight on photoanode synthesis for photoelectrochemical OER and offers a guidance on future electrocatalyst design.

INTRODUCTION

Hydrogen is an ideal energy carrier to address growing energy crises and environmental issues, benefiting from its carbon-neutral nature and high specific energy density. Electrochemical water splitting provides an appealing strategy for H_2 production under the ambient condition, where clean H_2O is applied as hydrogen source during the whole process.[1] However, the efficiency of water splitting is greatly hindered by oxygen evolution reaction (OER), which is caused by the sluggish kinetics of four proton/electron-coupled transfer process.[2, 3] To overcome the bottleneck reaction of water splitting, it requires us to develop superior OER electrocatalysts that can attain ultra-high OER current density under low overpotential. More importantly, it is more promising and attractive when the OER electrocatalysts can absorb other forms of external energy and couple the energy with electrochemical OER process for promoted OER kinetics under reduced power consumption.[3-6] Photo-coupled electrochemical OER is regarded as an effective method to enhance the electrochemical OER efficiency by harvesting solar energy.[7-10] First, it utilizes renewable energy to overcome high energy barrier of multi-step OER, thus reducing the dependence on electricity. Second, photo-generated holes induced by irradiation can also indirectly participate in oxidation process by producing highly oxidizing species, which can further improve

OER kinetics.[11] By designing an efficient OER electrocatalyst that can efficiently harvest light, it is of great promise to achieve robust OER performance with minimum electricity consumption.

CoS_2 is widely regarded as a great OER electrocatalyst due to OER-favourable oxidation state of Co and local environment around metal sites.[12] Meanwhile, CoS_2 is also known as a typical semiconductor with a narrow band gap of 2.2 eV,[13] which implies the underlying potential of CoS_2 to act as photo-coupled electrochemical electrode. However, the photo-responsible range of bare CoS_2 is still limited to light wavelength smaller than 563 nm, leading to a great loss of absorption in visible region of interest. Thus, it is a challenging issue to enhance the electrochemical OER activity of CoS_2 as well as extending its photoactivation response.

Local environment of metal ions is key in determining OER performance. Researchers have implemented strategies such as introducing nanointerface and alloying with another metal to modulate it.[14, 15] Other than that, doping is also a commonly used method to enhance the OER activity of metal center through synergistic chemical coupling effects between dopants and metal ions.[16] Furthermore, dopants can contribute to impurity levels located in the forbidden energy band, thus reducing the absorption energy.[17]

In this work, we synthesized N-doped CoS_2 nanorod arrays containing trace amount of Fe (N, Fe-CoS_2) on stainless steel (SS) photoanode. Fe from the substrate was incorporated into the sample during the synthesis of precursor. N atoms serve as dominant dopants that enhance intrinsic OER activity by manipulating the charge distribution and electronic structure of active sites. Introducing N atoms into lattice structure also engineer the effective band gap of a semiconductor by creating intermediate level between band gap, which can reduce the excitation energy and effectively extend the region of photoresponse to visible region. Moreover, it is reported that

oxidized Fe impurities resulting from the oxidization of Co sites also play a role in promoting OER activity, including enhancing conductiivty, reducing absorption energy of O-containing intermediates and promoting more charges to participate in OER reaction.[18-22] As expected, the CoS_2 anode shows enhanced electrochemical OER performance and improved photo-coupled electrochemical OER performance after modifying with N and Fe dopants. The N, Fe-CoS_2/SS anode reaches an intensive current density of 770 mA cm^{-2} under an overpotential of 350 mV in dark condition, which is approximately 4 times more than the value of Fe-CoS_2/SS. The excellent OER activity can be attributed to the increased number of active sites, improved conductivity and intrinsic activity induced by N, Fe-co-doping. Notably, when exposed to visible-NIR light illumination (>420 nm), the photoanode exhibits a distinct photoresponse, which is over 10 times more than that of Fe-CoS_2. This work not only provides an effective strategy to enhance electrochemical OER performance and increase light absorption of CoS_2, but also paves a new way to design high-efficient photoelectrochemical OER electrode.

EXPERIMENTAL SECTION

Materials: $CoCl_2 \cdot 6H_2O$ (98%) and sulfur powder were purchased from Alfa Aesar. Urea was obtained from Macklin. Ammonia solution (25%) was purchased from Baishi Chemical Co. Ltd. KOH was purchased from Sigma Aldrich. NH_4NO_3 was purchased from Kermel.

Synthesis of Materials: SS mesh was ultrasonically cleaned in de-ionized water, acetone, IPA and treated in 3 M HCl for 10 minutes, 1 hour, 30 minutes and 10 minutes accordingly in advance. The SS mesh was rinsed and then added to the pre-heated solution for 5 hours at 85 ℃.

$Co(OH)_2$ was directly synthesized onto stainless steel (SS) mesh using chemical bath deposition[23]. Specifically, 5 mmol of $CoCl_2 \cdot 6H_2O$ and 2.5 mmol of NH_4NO_3 were added to a flask together with 35 mL of de-ionized water and 5 mL of 25 % ammonia. The as-prepared solution was stirred in air for 10 minutes, and pre-heated at 85 ℃ for 30 minutes. The obtained precursor was rinsed and dried, then subjected to sequential sulfidation and doping processes to synthesize N, Fe-CoS_2.

In the sulfidation process, Fe-$Co(OH)_2$/SS and sulfur powder (0.5 g) were placed separately in a fused silica tube, and sulfur powder was at upstream side. Subsequently, the fused silica tube was heated to 350℃for 2 h with a heating rate of 2 ℃/min with the presence of Ar. The doping process was done using the same setup. This time, we placed urea (0.5 g) at upstream side and the fused silica tube was heated to 300 ℃ for 2 h with a heating rate of 5 ℃/min under Ar.

Characterization: Crystal structure of as-prepared samples were characterized by Rigaku SmartLab X-ray diffractometer using Cu Kα radiation. Morphology and structure of the synthesized materials were characterized using JEOL field-emission scanning electron microscopy (FESEM) at an accelerating voltage of 200.00 kV and JEOL Model JEM-2100F field emission electron microscope STEM. Samples for STEM were prepared by peeling off the active materials from substrate via 2-h sonication in ethanol. A drop of suspension was dropped on a piece of copper grid and dried in the air. Raman microscopy was conducted on as-synthesized sample using LabRAM HR 800 Raman Spectrometer fitted with 532 nm excitation laser. AMICUS ESCA 3400 X-ray photoelectron spectroscopy (XPS) was used to determine chemical compositions of materials using Al Kα 1486.6 eV radiation. Co L-edge X-ray absorption spectroscopy (XAS) measurements were performed at the beamline BL12B-a of the National Synchrotron Radiation Laboratory (NSRL) in Hefei, China. The electron beam energy of the storage ring was 800 MeV

with a maximum stored current of 300 mA. A bending magnet was connected to the beamline and equipped with three gratings covering photon energies from 100 to 1,000 eV with an energy resolution of ~0.2 eV. All of data were recorded in the total electron yield (TEY) mode by collecting the sample drain current under a vacuum greater than 5×10^{-8} Pa.

Electrochemical Measurements: Electrochemical measurements were conducted on CHI 614D electrochemical workstation. All measurement were performed using three-electrode configuration at ambient temperature in 1.0 M KOH. The as-synthesized N, Fe-CoS_2 was directly used as working electrode and a graphite rod was used as the counter electrode. The reference electrode was Hg/HgO. All the measured values were converted into reversible hydrogen electrode potential (RHE). Electrochemical impedance spectroscopy (EIS) spectra were obtained at open circuit potential in the frequency range from 10^{-2} Hz to 100 kHz. Photoelectrochemical OER performances were measured with the presence of simulated sunlight (100 mW cm^{-2}) with light wavelength of 420 nm and below filtered out.

RESULTS AND DISCUSSION

N, Fe-CoS_2/SS was prepared by chemical bath deposition followed by sulfidation and nitridation process using Fe-doped $Co(OH)_2$ (Fe-$Co(OH)_2$) as precursor, as illustrated in **Figure 1**(a). SEM images of precursor (Figure S1) present a large number of nanorods with an average length of 10 μm evenly distributing on stainless steel mesh (SS). The vertically aligned nanorod arrays offer open channels for electrolyte access and also increase the electrochemical surface area for O_2 evolution.[24] X-ray diffraction (XRD) pattern of precursor (Figure S2) validates the successful synthesis of well-crystallized $Co(OH)_2$ with strong and typical diffraction peaks (PDF#

30-443). We observed that all XRD peaks exhibit negative shifts compared with pristine $Co(OH)_2$, which can be attributed to Fe incorporation induced by replacement reaction between Co^{2+} and SS substrate during chemical deposition process.[19] According to the XRD peaks shift, the intercalation of Fe atoms expands crystal lattice due to a larger diameter of Fe than that of Co atoms. The photoelectron spectroscopy (XPS) profiles of precursor (Figure S3) further confirm the presence of Fe dopants. The high-resolution Fe 2p peak can be fitted into three peaks at the binding energy of 711.0 eV, 714.7 eV and 718.9 eV, corresponding to Fe^{2+} $2p_{3/2}$, Fe^{3+} $2p_{3/2}$, and satellite peak, respectively.[21] The high-resolution XPS spectrum of Co 2p contains two main peaks located at 780.6 eV, 795.9 eV, corresponding to $2p_{3/2}$ and $2p_{1/2}$ with their satellite peaks (at 805.3 eV and 790.3 eV). The Co $2p_{3/2}$ and Co $2p_{1/2}$ spin-orbit splitting value is 15.3 eV, suggesting the coexistence of Co^{2+} and Co^{3+}.[2] The presence of high valence states of Co^{3+} may result from oxidation of Co^{2+} promoted by Fe dopant.[25]

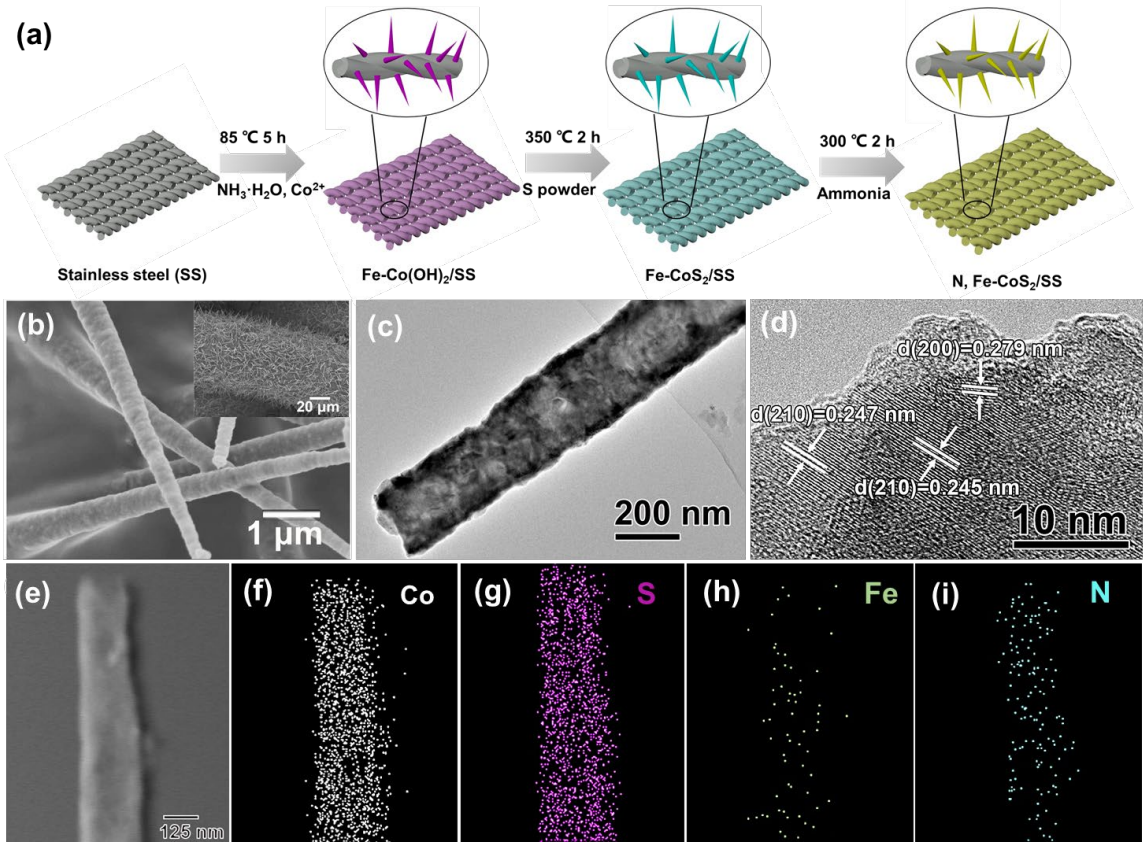

Figure 1. (a) Schematic diagram of the preparation of N, Fe-CoS_2 nanoarrays on SS mesh. (b) SEM images of N, Fe-CoS_2. (c) TEM image of N, Fe-CoS_2 nanorod. (d) HRTEM image of N, Fe-CoS_2 with d spacings indexed to (210) and (200) planes. (e)-(i) TEM element mapping of N, Fe-CoS_2 nanorod.

N, Fe-CoS_2/SS was synthesized by treating the as-prepared precursor via sulfidation and nitridation processes. According to SEM (Figure 1(b) and Figure S4) and transmission electron microscope (TEM) images (Figure 1(c)), the vertically aligned nanorod morphology is still well maintained, which enables facilitated electrolyte diffusion.[4] High-resolution transmission electron microscope (HRTEM) images (Figure 1(d)) shows distinct lattice fringes of N, Fe-CoS_2 are 0.247 nm and 0.279 nm, which are indexed to (210), (200) planes of CoS_2. It is noteworthy that the values of spaces of lattice fringe are slightly larger than the values of CoS_2, which should originate from the lattice expansion induced by Fe dopant.

XRD pattern (**Figure 2**(a)) confirms the successful conversion of N, Fe-CoS_2, as the new peaks agree well with typical XRD peaks of CoS_2 (PDF# 19-362). The peak positions of N, Fe-CoS_2 at 2θ=32.2°, 36.2°, 39.8°, 46.3°, 54.9° are corresponding to (200), (211), (210), (220), (311) planes of CoS_2 phase, respectively. All peaks of N, Fe-CoS_2 exhibit negative shifts compared with Fe-doped CoS_2 (Fe-CoS_2) (Figure 2(b)), which can be attributed to interstitial intercalation of N dopants.

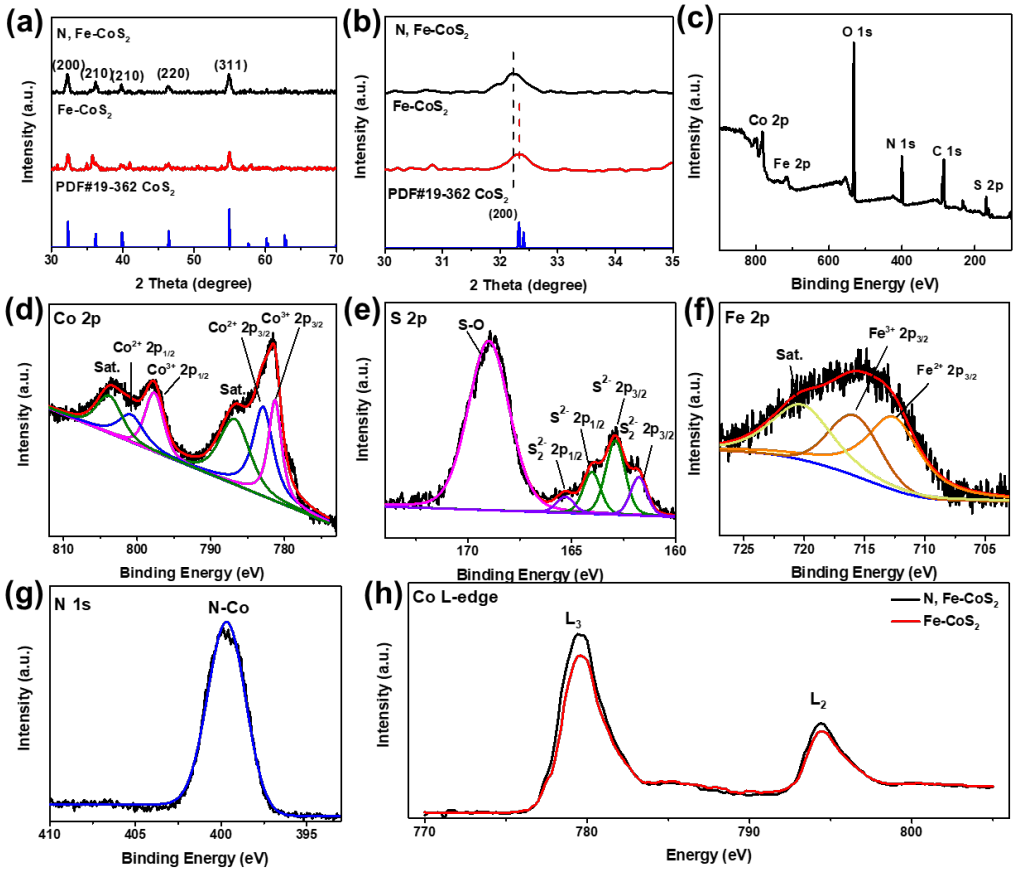

Figure 2. (a) XRD pattern of N, Fe-CoS_2 and Fe-CoS_2. (b) Enlarged peak at 2θ=32.2°. (c) XPS survey of N, Fe-CoS_2 nanorods. (d)-(g) Co 2p, Fe 2p, S 2p and N 1s high resolution spectra of N, Fe-CoS_2 (A) and Fe-CoS_2 (B). (h) XANES spectra of Co L-edge absorption for Fe-CoS_2 and N, Fe-CoS_2.

The survey XPS (Figure 2(d)) depicts the surface composition of N, Fe-CoS_2/SS and the N content approximates to 2.74 at%, as given in Table S1. Figure 2(e) shows that the Co 2p of N, Fe-CoS_2 splits into $2p_{3/2}$ and $2p_{1/2}$ doublets with characteristic satellite peaks (at 785.8 eV and 802.6 eV) on the side of these two signals. The peaks at 782.9 eV and 800.9 eV are identified to Co^{2+} species, and the peaks located at 781.2 eV and 797.6 eV are from oxidized Co^{2+}.[2] Gaussian fitting of Fe 2p peaks (Figure 2(f)) gives three peaks at 712.6 eV, 715.8 eV and 720.4 eV, corresponding to Fe^{2+} $2p_{3/2}$, Fe^{3+} $2p_{3/2}$ and satellite peak, respectively.[21] The high resolution of S 2p peak (Figure 2(g)) suggests three kinds of S signals, corresponding to S-O, S^{2-} and S_2^{2-} species.[3] The signal of S^{2-} can be ascribed to exposure to air, as reported in previous literature.[2, 12, 26] The S-O signal results from surface oxidization of sulfides in air.[27] The N 1s peak (Figure 2(h)) located at 399.8 eV corresponds to Co-N bond, indicating that N atoms are successfully doped into CoS_2 matrix.[2] Compared with Fe-CoS_2 (Fig. S5), Co 2p, Fe 2p and S 2p peaks of N, Fe-CoS_2 show positive shifts, which can be attributed to higher electronegativity of nitrogen impurities.[2, 3, 27, 28] The high electronegativity of nitrogen allows more electron occupation near N atom, thus enabling strong electron donation from N, Fe-CoS_2 to SS and providing preferable sites for proton discharge.[2, 29] Energy-dispersive X-ray (EDX) spectroscopy mapping results were collected to study the elemental distribution of N, Fe-CoS_2 nanorod. The elemental mapping images (Figure 1(e)-(i)) show that Co, Fe, N and S are uniformly distributed on the entire nanorod. EDX spectrum (Figure S6) illustrate the presence of Co, Fe, S, N. The results confirm the successful synthesis of N, Fe-CoS_2 on SS.

The electronic structure and local chemical environment of N, Fe-CoS_2 and Fe-CoS_2 were studied with X-ray absorption spectroscopy (XAS). Cobalt L-edge XAS spectra (Figure 2(c)), which probes primarily the *2p-3d* transitions, offers a quantitative information about the possibility

of the excitation from *2p* orbital to *3d* unoccupied states.[30] The Co L-edge splits into two peaks at 780 eV and 795 eV, corresponding to the L_3- and L_2-adsorption due to spin-orbit interaction of the Co $2p_{3/2}$ and $2p_{1/2}$ core states. The higher Co L_3 and L_2 intensity of N, Fe-CoS_2 compared with Fe-CoS_2 indicates that more vacancies are present in *3d* states of Co ions.[31, 32] This result directly confirms that N atoms manipulate the charge distribution and electronic structure around Co ions. It also reveals a stronger electron transfer from N, Fe-CoS_2 to SS. Due to the fact that d-band of transition metal ions affect the oxygen-related intermediates adsorption,[29, 31, 33] the N-modified unoccupied d-orbital density of Co ions in N, Fe-CoS_2 modulates the oxygen-surface interaction, resulting in enhanced OER activity and kinectics.

The as-prepared materials were directly used as working electrode for electrochemical measurements in alkaline solution (1.0 M KOH) at room temperature using standard three-electrode configuration. All polarization curves were obtained at a scan rate of 2 mV s^{-1} after iR-compensation. As suggested in the polarization curves (**Figure 3**(a)), the OER performance of Fe-CoS_2/SS is significantly enhanced by N dopants. From Figure 3(b), N, Fe-CoS_2/SS requires an overpotential of 215 mV to afford a current density of 10 mA cm^{-2}, while the values for Fe-CoS_2/SS and SS are 269 mV and 346 mV, respectively. Notably, when an overpotential of 350 mV is applied, the N, Fe-CoS_2/SS electrode achieves a pronounced current density of 770 mA cm^{-2}, while Fe-CoS_2/SS and SS can only achieve a current density of 200 mA cm^{-2} and 12 mA cm^{-2}, respectively. The ultra-high current density under a small potential reported in our work is much higher than the values reported for similar kinds of cobalt-based OER electrocatalysts (Table S2). Tafel slopes of N, Fe-CoS_2/SS, Fe-CoS_2/SS and SS are derived to investigate the effect of N doping on OER kinetics, as shown in Figure 3(c). A Tafel slope of 43.2 mV dec^{-1} is obtained for N, Fe-CoS_2/SS, which is much smaller than those of SS (70.7 mV dec^{-1}) and Fe-CoS_2/SS (56.0 mV dec-

[1]). The much reduced Tafel slope of N, Fe-CoS_2/SS confirms faster OER kinetics, indicating the significantly improved OER performance by N dopants.

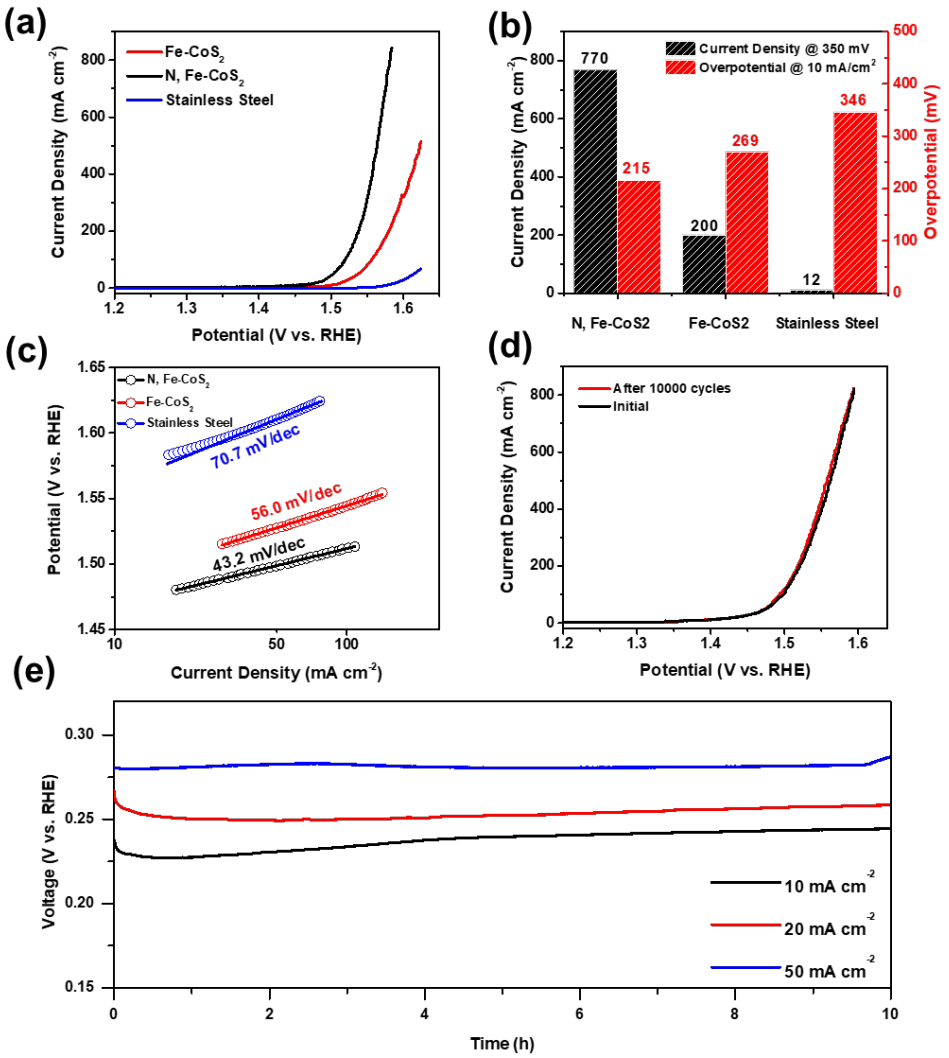

Figure 3. (a) Polarization curves of N, Fe-CoS_2, Fe-CoS_2 and stainless steel in 1.0 M KOH at scan rate of 2 mVs^{-1}. All curves are corrected with i-R compensation. (b) Current densities at 350 mV overpotential and overpotentials required to reach current density of 10 mA cm^{-2}. (c) Tafel slope of N, Fe-CoS_2, Fe-CoS_2 and stainless steel in 1.0 M KOH. (d) Polarization curves of N, Fe-CoS_2 before and after 10,000 cycles. (e) Long-term stability measurement of N, Fe-CoS_2 measured at current densities of 10 mA cm^{-2}, 20 mA cm^{-2} and 50 mA cm^{-2}.

The stability of our as-prepared electrocatalyst is evaluated through recycling test. As shown in Figure 3(d), a negligible decay of OER performance before and after 10,000 cycles suggests long-term stability of the as-synthesized electrode under 1.0 M KOH. In addition, insignificant catalytic activity decay (Figure 3(e)) is observed after 10 h of operation at current densities of 10 mA cm^{-2}, 20 mA cm^{-2} and 50 mA cm^{-2}, respectively. Thus, the as-prepared N, Fe-CoS_2/SS exhibits robust electrochemical OER performance and excellent long-term OER stability.

Electrochemical impedance spectroscopy (EIS) (Figure 4(a)) reveals a reduced charge transfer resistance (R_{ct}) of N, Fe-CoS_2/SS, compared with Fe-CoS_2/SS, at high frequency range. Lower R_{ct} suggests that N, Fe-CoS_2/SS has a better electrocatalyst-electrolyte contact than Fe-CoS_2/SS and therefore a greater capability of transporting electrons between electrode and electrolyte benefiting from N doping. At low frequency range, the steeper slope of N, Fe-CoS_2/SS suggests more sufficient electrolyte diffusion.[34, 35] The accelerated charge transfer kinetics and increased electrolyte interaction induced by N doping benefit the electrochemical OER process. The number of electrochemical surface area active sites (ECSA) was then estimated based on electrochemical double layer capacitances (C_{dl}).[36] The estimated C_{dl} of N, Fe-CoS_2/SS and Fe-CoS_2/SS were calculated by plotting current density against scan rate at 0.98 V (vs. RHE) from cyclic voltammetry curves (Figure S7). The results are presented in Figure 4(b). In Figure 4(c), the calculated C_{dl} values for N, Fe-CoS_2/SS and Fe-CoS_2/SS are 64.43 mF cm^{-2} and 45.74 mF cm^{-2}, corresponding to ECSA values of 1,610.75 cm^2 and 1,143.5 cm^2, respectively. We also determined the intrinsic activity of catalytic sites by normalizing current densities with ECSA. As suggested in Figure S8, N, Fe-CoS_2/SS still shows improved OER activity per catalytic site than pristine Fe-CoS_2/SS. Therefore, the above results illustrate that the excellent OER performance of Fe-CoS_2/SS

results from not only increased amount of active sites, but also improved conductivity and enhanced intrinsic activity induced by N doping.[2, 3]

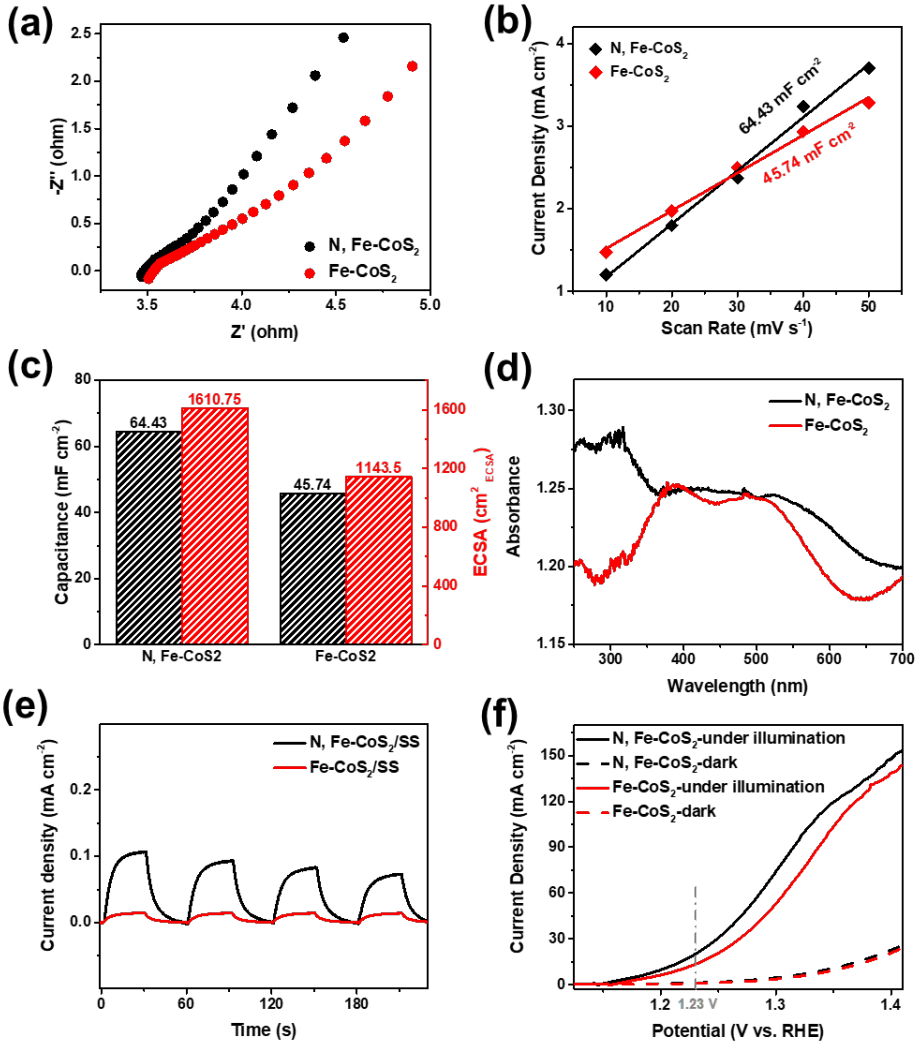

Figure 4. (a) Nyquist plots of N, Fe-CoS_2 and Fe-CoS_2. (b) The estimated value of C_d from plot of current density against different scan rates. (c) The estimated values of C_d and electrochemical surface area (ECSA) of N, Fe-CoS_2 and Fe-CoS_2. (d) Adsorption spectra of N, Fe-CoS_2 and Fe-CoS_2 nanorod arrays on stainless steel. (e) Photocurrent versus time curves performed with light on/off cycles at a potential of +0.1 V for N, Fe-CoS_2 and Fe-CoS_2. (f) Polarization curves of N, Fe-CoS_2 and Fe-CoS_2 measured under illumination

(solid line) and in the dark condition (dash line) in 1.0 M KOH solution with the presence of 1.0 M Na_2SO_3 as hole scavenger.

It has been reported that N and Fe doping can significantly broaden the light absorption, leading to red-shift in light absorption wavelength.[17, 37-39] Thus, we investigated the photoelectrochemical OER performance of our as-prepared N, Fe-CoS_2/SS in alkaline solution (1.0 M KOH) with the presence of 1.0 M Na_2SO_3 as hole scavenger at room temperature. We first confirmed the increase of light absorption caused by doping effect using ultraviolet visible light spectroscopy (UV-Vis). From Figure 4(d), the light absorption of N, Fe-CoS_2/SS in visible range is significantly enhanced compared with Fe-CoS_2/SS, implying the successful extension of photoactivation response of CoS_2 to visible-NIR region. The red shift in wavelength suggests a change in the electronic band gap level.[40] In order to investigate the band gap, we used the Kubelka-Munk function to calculate the band gap of N, Fe-CoS_2/SS and Fe-CoS_2/SS. As shown in Figure S13, the corresponding band gap values are 1.90 eV and 2.02 eV for N, Fe-CoS_2/SS and Fe-CoS_2/SS, respectively. The decrement of the band gap after doping process indicates N-modified electronic strucuture of Fe-CoS_2/SS, which may due to the introduction of defect states within the band gap.[28] The photoresponse of our samples to visible-NIR illumination was then recorded by photocurrent density versus time curve with light on/off cycle at +0.1 V (vs. Hg/HgO) in 1.0 M KOH. As shown in Figure 4(e), the photocurrent density of N, Fe-CoS_2/SS is approximately 10 times higher than that of Fe-CoS_2/SS upon illumination, confirming the enhanced photoresponse by N dopants and more photo-generated carriers induced by N dopants. Apart from light harvesting efficiency and spectra response, photogenerated carriers also play an important role in photoelectrochemical OER process.[41] Thus, we used Na_2SO_3 to capture the photogenerated holes to estimate the photoelectrochemical performance of as-prepared samples.

The fast sulfite oxidation kinetics enables itself occur prior to OER under theoretical potential for OER (1.23 V) or below.[42-44] As shown in Figure 4(f), the photocurrent density for N, Fe-CoS2/SS is 28.27 mA cm^{-2} at 1.23 V (vs. RHE) while the value for Fe-CoS_2 is 1.15 mA cm^{-2}. N, Fe-CoS_2 shows a dramatically increased current density than Fe-CoS_2, indicating better photoelectrochemical performance of N-doped electrode. Besides, the current density of N, Fe-CoS_2 experiences larger increase under illumination than that of Fe-CoS_2, further proving enhanced light absorption and improved charge transfer kinetics induced by N-doping is critically important in photo-couple electrochemical reaction. The abovementioned results suggest an indispensable role of N dopants in narrowing the effective band gap, improving the light harvesting ability, expediting interfacial kinetics and subsequently improving photoelectrochemical performance in visible range.

To further understand the OER mechanism of N, Fe-CoS_2, post-reaction characterizations were conducted to reveal the morphology and composition of the electrocatalyst after OER in dark condition. SEM results (Figure S9) show that the nanorod-morphology still maintains after the OER process in spite of the roughness induced by electrolysis, manifesting its high durability. We also investigated strucure change of post-reaction product using XRD. As shown in Figure S10, no characterisitc XRD peaks from CoS_2 can be observed from post-reaction product, suggesting that N, Fe-CoS_2 was converted into amorphous state after OER reaction. The amorphous state provides abundant defects which increases the amount of active sites, resulting in enhanced OER performance.[19] From Figure S12, the post-reaction product shows a prominently larger C_{dl} and ECSA than that of precursor. These results suggest that the oxidization process roughens the surface of nanorods and thus expose additional active sites compared with crystalline Fe-$Co(OH)_2$. In XPS survey (Figure S11), the disappearance of S species indicates the surface oxidization of N,

Fe-CoS_2 into cobalt hydroxide/oxyhydroxide during the OER process. High resolution of O 1s spectrum (Figure S11) is fitted into two separate peaks at 530.3 eV and 531.3 eV, attributing to lattice oxygen species and hydroxide species, respectively.[45] The N 1s window shows two peaks at 399.0 eV and 402.0 eV corresponding to N-Co and N-O bond, respectively.[46] The separation of the N 1s region reflects a change in chemical conditions after OER process.[47] The formation of hydroxide/oxyhydroxide is further supported by Raman spectroscopy result. As shown in Figure S11(e), the Raman bands at 479 and 685 cm^{-1} peaks manifest the Fe-OH/Co-OH symmetry mode ($A_{1g(T)}$) and Fe-O/Co-O symmetric stretching mode (A_g), respectively.[48] The S species here serve as scaffolds to form amorphous hydroxide/oxyhydroxide, which modifies the surface states of N, Fe-CoS_2 nanorods and act as active species during OER.

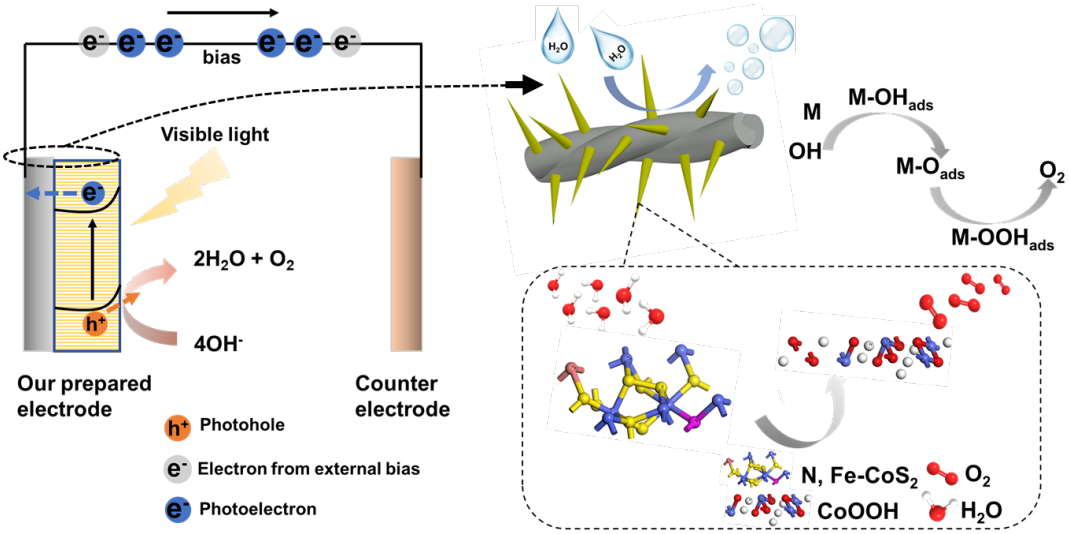

Figure 5. Schematic illustration of the photo-coupled electrochemical OER mechanism of N, Fe-CoS_2/SS.

Figure 5 illustrates the photoelectrochemical OER mechanism on the N, Fe-CoS_2/SS photoanode. Upon illumination, photo-generated electron-hole pairs are separated and transported to the surface of electrocatalyst to participate in surface redox reaction.[49] Meanwhile, photoelectrons are transferred to the counter electrode to generate hydrogen. The generation of

photogenerated-carriers creates a driving potential, which subsidizes the external bias required to occur oxygen evolution and thus reduce the overpotential. Holes also play a role in generating hydroxyl radicals, which are reactive oxidants for oxygen evolution.[11] Therefore, the OER kinetics can be further enhanced. As severe photogenerated-electron/hole recombination deteriorates the efficiency of light harvesting, a positive external bias hinders the recombination by accelerating hole and electron diffusion to the electrode/solution interface.[50] The nanorod structure is also beneficial to overcome the short diffusion length of photo-generated holes and to restrain recombination.[49] During the OER process, a thin layer of CoOOH, which is formed at the surface of N, Fe-CoS_2 nanorods during OER, serves as the active material for oxygen evolution.[4]

CONCLUSIONS

In summary, we demonstrate N, Fe-CoS_2 nanorods on stainless steel mesh as robust OER electrocatalyst and remarkable photo-coupled electrochemical OER catalyst in alkaline environment with excellent stability. The anode demonstrates a low overpotential of 215 mV at 10 mA cm^{-2} and an intensive current density of 770 mA cm^{-2} under an overpotential of 350 mV. More importantly, N doping improves the light absorption and extends the photoresponse of Fe-CoS_2 to visible region, greatly improving the photoelectrochemical performance. These results manifest the great possibility of N, Fe-CoS_2/SS electrode for serving as a high-efficient photoelectrochemical OER anode. This study highlights an effective and novel strategy for photoelectrochemical OER electrode design by introducing doping manipulation, which is beneficial for PEC anode development.

ASSOCIATED CONTENT

Supporting Information. The following files are available free of charge.

Characterization, electrical property measurement of the as-prepared electrodes (docx)

AUTHOR INFORMATION

Corresponding Author

*Email: ychai@polyu.edu.hk

Notes

There are no conflicts to declare.

ACKNOWLEDGMENT

J. Y. L. and L. J. C. contributed equally to this work. This research work was supported by the Hong Kong Polytechnic University (G-YW2A). We thank the beamline BL12B-a of the National Synchrotron Radiation Laboratory (NSRL) in Hefei, China for Co L-edge XAS measurements.

REFERENCES

1. Riis, T.; Hagen, E. F.; Vie, P.; Ulleberg, Ø., Hydrogen Production and Storage—R&D Priorities and Gaps. *IEA Hydrogen Implementing Agreement (HIA), International Energy Agency (IEA), Paris* **2006**.

2. Hao, J.; Yang, W.; Peng, Z.; Zhang, C.; Huang, Z.; Shi, W., A Nitrogen Doping Method for CoS_2 Electrocatalysts with Enhanced Water Oxidation Performance. *ACS Catal.* **2017,** *7* (6), 4214-4220.

3. Hao, J.; Yang, W.; Hou, J.; Mao, B.; Huang, Z.; Shi, W., Nitrogen Doped NiS_2 Nanoarrays with Enhanced Electrocatalytic Activity for Water Oxidation. *J. Mater. Chem. A* **2017,** *5* (34), 17811-17816.

4. Chen, P.; Xu, K.; Fang, Z.; Tong, Y.; Wu, J.; Lu, X.; Peng, X.; Ding, H.; Wu, C.; Xie, Y., Metallic Co_4N Porous Nanowire Arrays Activated by Surface Oxidation as Electrocatalysts for the Oxygen Evolution Reaction. *Angew. Chem. Int. Ed.* **2015,** *54* (49), 14710-14714.

5. Zhang, B.; Lui, Y. H.; Ni, H.; Hu, S., Bimetallic $(Fe_xNi_{1-x})_2P$ Nanoarrays as Exceptionally Efficient Electrocatalysts for Oxygen Evolution in Alkaline and Neutral Media. *Nano Energy* **2017,** *38*, 553-560.

6. Liu, W.; Liu, H.; Dang, L.; Zhang, H.; Wu, X.; Yang, B.; Li, Z.; Zhang, X.; Lei, L.; Jin, S., Amorphous Cobalt-Iron Hydroxide Nanosheet Electrocatalyst for Efficient Electrochemical and Photo-Electrochemical Oxygen Evolution. *Adv. Funct. Mater.* **2017,** *27* (14), 1603904.

7. Zheng, Y.; Wang, W.; Jiang, D.; Zhang, L.; Li, X.; Wang, Z., Ultrathin Mesoporous Co_3O_4 Nanosheets with Excellent Photo-/Thermo-catalytic Activity. *J. Mater. Chem. A* **2016,** *4* (1), 105-112.

8. Ruff, T.; Hahn, R.; Killian, M. S.; Asoh, H.; Ono, S.; Schmuki, P., Visible Light Photo Response from N-doped Anodic Niobium Oxide after Annealing in Ammonia Atmosphere. *Electrochim. Acta* **2011,** *62*, 402-407.

9. Hou, Y.; Zhuang, X.; Feng, X., Recent Advances in Earth-Abundant Heterogeneous Electrocatalysts for Photoelectrochemical Water Splitting. *Small Methods* **2017,** *1* (6), 1700090.

10. Wang, H.; Wu, Y.; Yuan, X.; Zeng, G.; Zhou, J.; Wang, X.; Chew, J. W., Clay-Inspired MXene-Based Electrochemical Devices and Photo-Electrocatalyst: State-of-the-Art Progresses and Challenges. *Adv. Mater.* **2018,** *30* (12), 1704561.

11. Hoffmann, M. R.; Martin, S. T.; Choi, W.; Bahnemann, D. W., Environmental Applications of Semiconductor Photocatalysis. *Chem. Rev.* **1995,** *95* (1), 69-96.

12. Ma, X.; Zhang, W.; Deng, Y.; Zhong, C.; Hu, W.; Han, X., Phase and Composition Controlled Synthesis of Cobalt Sulfide Hollow Nanospheres for Electrocatalytic Water Splitting. *Nanoscale* **2018,** *10* (10), 4816-4824.

13. Soofivand, F.; Sabet, M.; Seyghalkar, H.; Salavati-Niasari, M., Using the $[Co(oct)_2]$ as a New Precursor for Simple Synthesis of CoS_2 Nanoparticles and Kinetics Studies on Photocatalytic Activities Under UV Irradiation. *J. Nanostruct.* **2018,** *8* (1), 75-81.

14. Qiu, B.; Cai, L.; Wang, Y.; Ma, S.; Tsang, Y. H.; Chai, Y., Accelerated Oxygen Evolution Kinetics on Nickel–Iron Diselenide Nanotubes by Modulating Electronic Structure. *Materials Today Energy* **2019,** *11*, 89-96.

15. Qiu, B.; Wang, C.; Zhang, N.; Cai, L.; Xiong, Y.; Chai, Y., CeO_2-Induced Interfacial Co^{2+} Octahedral Sites and Oxygen Vacancies for Water Oxidation. *ACS Catal.* **2019,** *9* (7), 6484-6490.

16. Peng, L.; Shah, S. S. A.; Wei, Z., Recent Developments in Metal Phosphide and Sulfide Electrocatalysts for Oxygen Evolution Reaction. *Chinese J. Catal.* **2018,** *39* (10), 1575-1593.

17. Yang, X.; Wolcott, A.; Wang, G.; Sobo, A.; Fitzmorris, R. C.; Qian, F.; Zhang, J. Z.; Li, Y., Nitrogen-doped ZnO Nanowire Arrays for Photoelectrochemical Water Splitting. *Nano Lett.* **2009,** *9* (6), 2331-2336.

18. Corrigan, D. A.; Conell, R. S.; Fierro, C. A.; Scherson, D. A., In-situ Moessbauer Study of Redox Processes in a Composite Hydroxide of Iron and Nickel. *J. Phys. Chem.* **1987,** *91* (19), 5009-5011.

19. Cai, L.; Qiu, B.; Lin, Z.; Wang, Y.; Ma, S.; Wang, M.; Tsang, Y. H.; Chai, Y., Active Site Engineering of Fe- and Ni-sites for Highly Efficient Electrochemical Overall Water Splitting. *J. Mater. Chem. A* **2018,** *6* (43), 21445-21451.

20. Li, N.; Bediako, D. K.; Hadt, R. G.; Hayes, D.; Kempa, T. J.; von Cube, F.; Bell, D. C.; Chen, L. X.; Nocera, D. G., Influence of Iron Doping on Tetravalent Nickel Content in Catalytic Oxygen Evolving Films. *Proc. Natl. Acad.. Sci U.S.A.* **2017,** *114* (7), 1486-1491.

21. Tang, C.; Gan, L.; Zhang, R.; Lu, W.; Jiang, X.; Asiri, A. M.; Sun, X.; Wang, J.; Chen, L., Ternary $Fe_xCo_{1-x}P$ Nanowire Array as a Robust Hydrogen Evolution Reaction Electrocatalyst with Pt-like Activity: Experimental and Theoretical Insight. *Nano Lett.* **2016,** *16* (10), 6617-6621.

22. Tang, C.; Zhang, R.; Lu, W.; He, L.; Jiang, X.; Asiri, A. M.; Sun, X., Fe‐doped CoP Nanoarray: a Monolithic Multifunctional Catalyst for Highly Efficient Hydrogen Generation. *Adv. Mater.* **2017,** *29* (2), 1602441.

23. Chen, Z.; Kronawitter, C. X.; Yeh, Y.-W.; Yang, X.; Zhao, P.; Yao, N.; Koel, B. E., Activity of Pure and Transition Metal-modified CoOOH for the Oxygen Evolution Reaction in an Alkaline Medium. *J. Mater. Chem. A* **2017,** *5* (2), 842-850.

24. Liu, J.; Zhu, D. D.; Zheng, Y.; Vasileff, A.; Qiao, S., Self-Supported Earth-Abundant Nanoarrays as Efficient and Robust Electrocatalysts for Energy-Related Reactions. *ACS Catal.* 2018, *8*(7), 6707-6732.

25. Zhou, T.; Cao, Z.; Wang, H.; Gao, Z.; Li, L.; Ma, H.; Zhao, Y., Ultrathin CoFe Hydroxide Nanosheet Arrays for Improved Oxygen Evolution during Water Splitting. *RSC Adv.* **2017,** *7* (37), 22818-22824.

26. Ning, H.; Liu, Z.; Xie, Y.; Huang, H., CoS_2 Coatings for Improving Thermal Stability and Electrochemical Performance of FeS_2 Cathodes for Thermal Batteries. *J. Electrochem. Soc.* **2018,** *165* (9), 1725-1733.

27. Ouyang, C.; Wang, X.; Wang, S., Phosphorus-doped CoS_2 Nanosheet Arrays as Ultra-efficient Electrocatalysts for the Hydrogen Evolution Reaction. *Chem. Commun. (Camb)* **2015,** *51* (75), 14160-14163.

28. Zhang, X.; Meng, F.; Mao, S.; Ding, Q.; Shearer, M. J.; Faber, M. S.; Chen, J.; Hamers, R. J.; Jin, S., Amorphous MoS_xCl_y Electrocatalyst Supported by Vertical Graphene for Efficient Electrochemical and Photoelectrochemical Hydrogen Generation. *Energy Environ. Sci.* **2015,** *8* (3), 862-868.

29. Gao, M.-R.; Cao, X.; Gao, Q.; Xu, Y.-F.; Zheng, Y.-R.; Jiang, J.; Yu, S.-H., Nitrogen-doped Graphene Supported $CoSe_2$ Nanobelt Composite Catalyst for Efficient Water Oxidation. *ACS Nano.* **2014,** *8* (4), 3970.

30. Kornienko, N.; Resasco, J.; Becknell, N.; Jiang, C.-M.; Liu, Y.-S.; Nie, K.; Sun, X.; Guo, J.; Leone, S. R.; Yang, P., Operando Spectroscopic Analysis of an Amorphous Cobalt Sulfide Hydrogen Evolution Electrocatalyst. *J. Am. Chem. Soc.* **2015,** *137* (23), 7448-7455.

31. Lu, T. H.; Chen, C. J.; Lu, Y. R.; Dong, C. L.; Liu, R. S., Synergistic-Effect-Controlled $CoTe_2$ /Carbon Nanotube Hybrid Material for Efficient Water Oxidation. *J. Phys. Chem. C* **2016,** *120* (49), 28093-28099.

32. Chen, C. J.; Chen, P. T.; Basu, M.; Yang, K. C.; Lu, Y. R.; Dong, C. L.; Ma, C. G.; Shen, C. C.; Hu, S. F.; Liu, R. S., An Integrated Cobalt Disulfide (CoS_2) co-Catalyst Passivation Layer on Silicon Microwires for Photoelectrochemical Hydrogen Evolution. *J. Mater. Chem. A* **2015,** *3* (46), 23466-23476.

33. Antonov, V.; Andryushchenko, O.; Shpak, A.; Yaresko, A.; Jepsen, O., Electronic Structure, Optical Spectra, and X-Ray Magnetic Circular Dichroism in CoS_2. *Phys. Rev. B* **2008,** *78* (9), 094409.

34. Balogun, M. S.; Qiu, W.; Huang, Y.; Yang, H.; Xu, R.; Zhao, W.; Li, G. R.; Ji, H.; Tong, Y., Cost-Effective Alkaline Water Electrolysis Based on Nitrogen- and Phosphorus-Doped Self-Supportive Electrocatalysts. *Adv. Mater.* **2017,** *29* (34), 1702095.

35. Qiu, B.; Cai, L.; Wang, Y.; Lin, Z.; Zuo, Y.; Wang, M.; Chai, Y., Fabrication of Nickel-Cobalt Bimetal Phosphide Nanocages for Enhanced Oxygen Evolution Catalysis. *Adv. Funct. Mater.* **2018,** *28* (17), 1706008.

36. Wu, H. B.; Xia, B. Y.; Yu, L.; Yu, X.-Y.; Lou, X. W., Porous Molybdenum Carbide Nano-Octahedrons Synthesized via Confined Carburization in Metal-organic Frameworks for Efficient Hydrogen Production. *Nat. Commun.* **2015,** *6* (1), 6512.

37. Ahn, K.-S.; Yan, Y.; Shet, S.; Deutsch, T.; Turner, J.; Al-Jassim, M., Enhanced Photoelectrochemical Responses of ZnO Films through Ga and N Codoping. *Appl. Phys. Lett.* **2007,** *91* (23), 231909.

38. Asahi, R.; Morikawa, T.; Ohwaki, T.; Aoki, K.; Taga, Y., Visible-light Photocatalysis in Nitrogen-doped Titanium Oxides. *Science* **2001,** *293* (5528), 269-271.

39. Yu, J.; Xiang, Q.; Zhou, M., Preparation, Characterization and Visible-light-driven Photocatalytic Activity of Fe-doped Titania Nanorods and First-principles Study for Electronic Structures. *Appl. Catal. B: Environ.* **2009,** *90* (3-4), 595-602.

40. Ganesan, P.; Prabu, M.; Sanetuntikul, J.; Shanmugam, S., Cobalt Sulfide Nanoparticles Grown on Nitrogen and Sulfur Codoped Graphene Oxide: An Efficient Electrocatalyst for Oxygen Reduction and Evolution Reactions. *ACS Catal.* **2015,** *5* (6), 3625-3637.

41. Ahmed, R.; Xu, Y.; Zangari, G., Water Splitting vs. Sulfite Oxidation: An Assessment of Photoelectrochemical Performance of TiO_2 Nanotubes Modified by CdS/CdSe Nanoparticles. *Electrochim. Acta* **2018,** *259*, 1095-1103.

42. Ibadurrohman, M.; Hellgardt, K., Photoelectrochemical Performance of Graphene-modified TiO_2 Photoanodes in the Presence of Glycerol as a Hole Scavenger. *Int. J. Hydrog. Energy* **2014,** *39* (32), 18204-18215.

43. Wei, P.; Lin, K.; Meng, D.; Xie, T.; Na, Y., Photoelectrochemical Performance for Water Oxidation Improved by Molecular Nickel Porphyrin-Integrated WO_3/TiO_2 Photoanode. *ChemSusChem* **2018,** *11* (11), 1746-1750.

44. Ye, X.; Yang, J.; Boloor, M.; Melosh, N. A.; Chueh, W. C., Thermally-enhanced Minority Carrier Collection in Hematite during Photoelectrochemical Water and Sulfite Oxidation. *J. Mater. Chem. A* **2015,** *3* (20), 10801-10810.

45. Yang, J.; Liu, H.; Martens, W. N.; Frost, R. L., Synthesis and Characterization of Cobalt Hydroxide, Cobalt Oxyhydroxide, and Cobalt Oxide Nanodiscs. *J. Phys. Chem. C* **2010,** *114* (1), 111-119.

46. Ren, Z.; Xu, X.; Wang, X.; Gao, B.; Yue, Q.; Song, W.; Zhang, L.; Wang, H., FTIR, Raman, and XPS Analysis during Phosphate, Nitrate and Cr (VI) Removal by Amine Cross-linking Biosorbent. *J. Colloid Interf. Sci.* **2016,** *468*, 313-323.

47. Zhang, K.; Xia, X.; Deng, S.; Zhong, Y.; Xie, D.; Pan, G.; Wu, J.; Liu, Q.; Wang, X.; Tu, J., Nitrogen-Doped Sponge Ni Fibers as Highly Efficient Electrocatalysts for Oxygen Evolution Reaction. *Nano-Micro Lett.* **2019,** *11* (1), 21.

48. Li, H. B.; Gao, Y. Q.; Yang, G. W., Electrochemical Route for Accessing Amorphous Mixed-metal Hydroxide Nanospheres and Magnetism. *RSC Adv.* **2015,** *5* (56), 45359-45367.

49. Jiang, C.; Moniz, S. J. A.; Wang, A.; Zhang, T.; Tang, J., Photoelectrochemical Devices for Solar Water Splitting - Materials and Challenges. *Chem. Soc. Rev.* **2017,** *46* (15), 4645-4660.

50. Jin, T.; Diao, P.; Wu, Q.; Xu, D.; Hu, D.; Xie, Y.; Zhang, M., WO_3 Nanoneedles/α-Fe_2O_3/Cobalt Phosphate Composite Photoanode for Efficient Photoelectrochemical Water Splitting. *Appl. Catal. B: Environ.* **2014,** *148-149*, 304-310.